JOURNAL OF SOLID STATE CHEMISTRY 51, 170–175 (1984)

# Photoelectronic Properties of $ReS_2$ and $ReSe_2$ Single Crystals

JAMES V. MARZIK, ROBERT KERSHAW, KIRBY DWIGHT, AND AARON WOLD*

*Department of Chemistry, Brown University, Providence, Rhode Island 02912*

Received June 23, 1983, and in revised form September 12, 1983

Large single crystals of $ReS_2$ and $ReSe_2$ were grown by chemical vapor transport and several of their properties were investigated. Both were found to be *n*-type semiconductors with resistivities in the range of 1–10 ohm-cm. Photoelectrochemical measurements in aqueous solutions of $I_3^-/I^-$ resulted in high photocurrent densities, with $ReSe_2$ being the more efficient photoelectrode. Analysis of their optical absorption spectra resulted in lowest-energy indirect optical band gaps of 1.32(5) eV for $ReS_2$ and 1.17(5) eV for $ReSe_2$. Photoelectrochemical spectral response measurements resulted in a measured lowest-energy indirect optical band gap of 1.4 eV for $ReS_2$, which is in close agreement with that measured from optical absorption.

## Introduction

In 1977, Tributsch reported the first photoelectrochemical studies of $MoS_2$ (*1–3*) and proposed the transition metal dichalcogenides as a new class of electrodes for electrochemical solar cells. Since then, these materials have been shown to be relatively stable and efficient as photoelectrodes, and there have been a number of photoelectrochemical studies of $MoS_2$, $MoSe_2$, $WS_2$, and $WSe_2$ (*4–23*) as well as other transition metal dichalcogenides (*24, 25*).

It is of interest in this laboratory to investigate layer-type semiconductors containing 4*d* and 5*d* transition metals as possible photoelectrodes and photocatalysts. Recently, PdPSe was reported (*26*) as the first observed photoactive semiconductor containing palladium. $ReS_2$ and $ReSe_2$ are both layer-type semiconductors (*27*), but there have not been any reported photoelectrochemical investigations of these materials.

Previous studies (*27, 28*) showed that $ReS_2$ and $ReSe_2$ are isostructural and possess triclinic symmetry. The anions form a distorted cubic close-packed array in which rhenium occupies pseudo-octahedral holes in every other layer. Thus, as in the $MoS_2$-type structure, there are anion–metal–anion sandwiches connected to one another by weak van der Waals' forces. Within one anion–metal–anion layer, each rhenium is shifted towards one face of its octahedron, giving three short and three long Re–Se bonds and three significantly short Re–Re distances. This results in the formation of $Re_4$ clusters connected to each other along the *b* direction by Re–Re bonds (see Fig. 1). The average bond distance within each $Re_4$ cluster is 2.83 Å, and each cluster is connected along the *b* direction with a 3.07-Å Re–Re bond. It has been suggested (*1, 2*)

* To whom all correspondence should be addressed.

0022-4596/84 $3.00

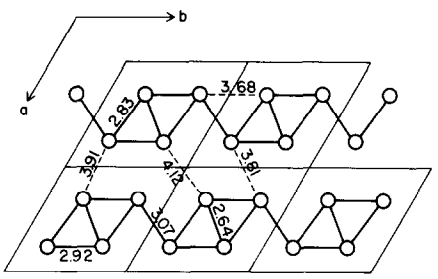


FIG. 1. Cation layer of the $ReSe_2$ structure approximately parallel to the (001) plane (anions are not shown). Metal–metal distances are in angstroms, and solid lines indicate metal–metal bonding. The diagram shows the formation of $Re_4$ clusters, which are connected to each other along the *b* direction by Re–Re bonds.

that transition metal dichalcogenides with short metal–metal distances should have optimal *d–d* band splitting and the most desirable properties for photoelectrochemical applications, and hence, it was of interest to investigate the properties of $ReS_2$ and $ReSe_2$.

## Experimental

*Synthesis.* Single crystals of $ReS_2$ and $ReSe_2$ were synthesized by chemical vapor transport using bromine. Rhenium (Shattuck 99.99%) was prereduced at 950°C under 85%/15% $Ar/H_2$ gas for 12 hr and then heated for 4 hr at 350°C under dynamic vacuum to remove any adsorbed hydrogen. Sulfur (Gallard–Schlesinger 99.999%) and selenium (Gallard–Schlesinger 99.999%) were freshly sublimed. Transport tubes containing bromine and stoichiometric amounts of the elements were prepared with an H-tube filling apparatus as previously described (*29*). The transport tube was placed in a three-zone furnace and the charge prereacted for 24 hr at 800°C with the growth zone at 1150°C, preventing transport of the product. The furnace was then equilibrated to give a constant temperature across the reaction tube, and was programmed over 24–48 hr to give the temperature gradient at which single crystal growth took place. Crystals grew in the cooler zone of the furnace with experiments generally running 5–7 days. A gradient of 1125–1075°C was used for $ReS_2$ and 1075–1025°C for $ReSe_2$. Both $ReS_2$ and $ReSe_2$ formed silver-colored, graphite-like, thin hexagonal platelets up to 1 $cm^2$ in area and 50 $\mu$m in thickness.

*X-ray analysis.* X-Ray diffraction patterns of single crystals were obtained using a Gandolfi camera (Blake Industries D1100) and Ni-filtered Cu$K\alpha$ radiation. The patterns confirmed the triclinic symmetry of $ReS_2$ and $ReSe_2$ with cell parameters consistent with those previously reported (*27*).

*TGA.* Thermogravimetric analysis was performed using a Cahn electrobalance (Model RG). The materials were reduced to the metal in a stream of hydrogen gas. Temperatures were programmed to 1000°C at a rate of 30°C/hr. The presence of single phase rhenium metal as the reduction product was confirmed by X-ray diffraction.

*Electrical measurements.* Resistivity and DC Hall effect were measured on single crystals using the van der Pauw technique (*30*). Contacts were made by the ultrasonic soldering of indium directly onto the samples, and ohmic behavior was established by measuring the current–voltage characteristics. The activation energy of resistivity $E_a$ (defined for semiconductors by $\rho = \rho_0 \exp(E_a/kT)$, where $\rho$ = resistivity, $\rho_0$ is a constant, $T$ = temperature (K), and $k$ = the Boltzmann constant) was determined by measuring $\rho$ as a function of $T$.

*Optical measurements.* Optical absorption of thin (5–25$\mu$m) single crystals was measured with a Cary 17 spectrophotometer. The absorption coefficient $\alpha$ was calculated from the transmission ratio $T$ using the exprestion $T = (1 - R)^2 e^{-\alpha t}/[1 - (R^2 e^{-2\alpha t})]$, where $t$ is the sample thickness and $R$ is the reflectivity calculated for the above expression by assuming $\alpha \simeq 0$ in the

part of the spectrum far removed from the absorption edge.

*Electrode preparation.* Photoelectrodes were prepared by evaporating thin films of gold on the backs of the single crystals of $ReS_2$ and $ReSe_2$ in order to provide good ohmic electrical contact. For mechanical support, the gold face of each crystal was affixed to a disk of platinum foil with a drop of silver paint. The platinum foil was soldered to a platinum wire which was sealed inside a Pyrex tube, and the electrode was rinsed with $CCl_4$ (Fischer Spectroanalyzed) and air dried. An insulating resin (Miccrostop, Michigan Chrome Chemical Corp.) was applied to the platinum foil and wire so that only the front surface of the crystal was in electrical contact with the electrolyte solution. Electrodes were rinsed with methanol (Fisher Certified Electronic Grade) and air-dried before each measurement.

*Photoelectrochemical measurements.* Photoelectrochemical measurements were carried out with a 150-W xenon lamp, a monochromator (Oriel 7240), a glass cell with a quartz window, and a current amplifier as previous described (*14*). A platinized platinum electrode was used as a counter electrode. Potential measurements were made with respect to a saturated calomel electrode (Fischer 13-639-56). For sampled current–potential measurements under steady-state conditions, bias was applied via a potentiometer and a voltage follower having a very low output impedance (<0.1 ohm). A tungsten iodide lamp was used for wavelength dependency measurements. The quantum efficiency was determined by dividing the current through the cell by the incident photon flux, measured with a calibrated Si photodiode (*14*).

Analyzed reagent grade chemicals and deionized water (18.3 MΩ) were used in order to minimize impurities in the electrolyte. The electrolyte used was an aqueous solution of 0.05 *M* NaI/0.002 *M* $I_2$/0.05 *M* $H_2SO_4$ which results in the $I_3^-/I^-$ couple as the electroactive species in solution. For the sampled current–potential measurements, the electrolyte was continuously bubbled with nitrogen gas. The rest potential of the electrolyte solution was 0.335 V versus SCE.

## Results and Discussion

X-Ray diffraction confirmed the triclinic symmetry of $ReS_2$ and $ReS_2$ with cell parameters consistent with those previously reported (*27*). Thermogravimetric analyses confirmed the stoichiometry of $ReS_2$ (wt% Re calculated: 74.4; found: 74.5(2)) and $ReSe_2$ (wt% Re calculated: 54.1; found: 54.4(2)).

The electrical properties of $ReS_2$ and $ReSe_2$ are summarized in Table I. Both materials were found to be *n*-type semiconductors with resistitivites in the range of 1–10 ohm-cm. Activation energies calculated from the temperature dependence of the resistivity were found to be close to those calculated from the temperature dependence of the carrier concentration obtained from Hall voltage measurements.

Figure 2 is a plot of $(\alpha h\nu)^{0.5}$ as a function of photon energy which results in lowest-

TABLE I

ELECTRICAL PROPERTIES OF $ReS_2$ AND $ReSe_2$

| | $ReS_2$ | $ReSe_2$ |
|---|---|---|
| Resistivity[a] | 3 ohm-cm | 8 ohm-cm |
| Carrier concentration[a] | $1 \times 10^{17}$ cm$^{-3}$ | $7 \times 10^{16}$ cm$^{-3}$ |
| Hall mobility[a] | 20 cm$^2$ V$^{-1}$ sec$^{-1}$ | 10 cm$^2$ V$^{-1}$ sec$^{-1}$ |
| Carrier type[b] | *n* | *n* |
| $E_{a(R)}$[c] | 0.06 eV | 0.21 eV |
| $E_{a(H)}$[d] | 0.08 eV | 0.25 eV |

[a] 298 K.

[b] Determined from DC Hall and qualitative Seebeck measurements.

[c] Activation energy calculated from the temperature dependence of the resistivity.

[d] Activation energy calculated from the temperature dependence of the carrier concentration (obtained from Hall voltage measurements).

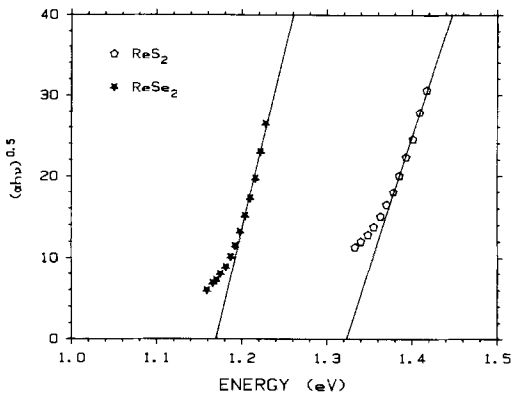


FIG. 2. Analysis of the optical absorption spectra of $ReS_2$ and $ReSe_2$ in the region of the absorption edge, giving indirect optical band gaps of 1.32(5) eV and 1.17(5) eV, respectively.

energy indirect optical band gaps of 1.32(5) eV for $ReS_2$ and 1.17(5) eV for $ReSe_2$. These are in agreement with previously reported values (*27*).

The photoresponses observed for $ReS_2$ and $ReSe_2$ single crystals from sampled current–potential measurements under steady-state conditions are shown in Fig. 3 where the photocurrents obtained in "white" light are plotted against the potential of the working electrode measured with respect to a saturated calomel electrode (SCE). The onset potential of photocurrent was approximately 0.0 V versus SCE for $ReS_2$ and −0.2 V versus SCE for $ReSe_2$ in aqueous solutions of $I_3^-/I^-$ (pH 1). Observed photocurrents for $ReSe_2$ were higher than those for $ReS_2$ although the electrode surfaces of both materials were generally of equal quality. This is consistent with the smaller optical band of $ReSe_2$ compared to $ReS_2$.

The quantum efficiency $\eta$ (in electrons/photon) measured at a working electrode potential of 0.335 V versus SCE is plotted versus wavelength in Fig. 4. Experiments showed negligible electrolyte absorption in this spectral region. The marked shift of the spectral response towards longer wavelengths indicates that $ReSe_2$ has a smaller band gap than $ReS_2$. This is consistent with an analysis of the optical absorption spectra of $ReS_2$ and $ReSe_2$ in the region of the absorption edge. Analysis of the photoelectrochemical spectral response data (*31*) results in a lowest-energy indirect optical band gap of 1.4 eV for $ReS_2$ which is in close agreement with that measured from the optical absorption spectrum. Such an analysis was not carried out for $ReSe_2$ because its absorption edge is in the same region as the absorption edge of the Si photodiode used to calculate quantum efficiencies.

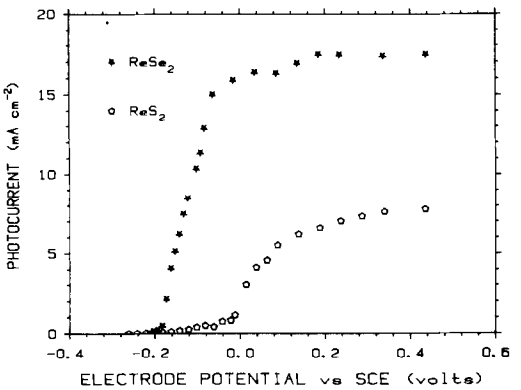


FIG. 3. Variation of photocurrent with electrode potential under "white" xenon arc irradiation of 1.0 W/cm² in an aqueous $I_3^-/I^-$ electrolyte solution.

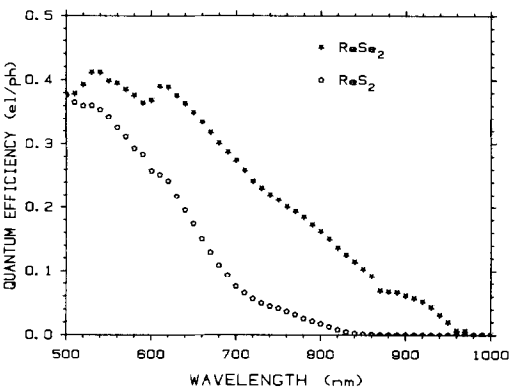


FIG. 4. Spectral variation of the quantum efficiency obtained at an electrode potential of 0.335 V versus SCE in an aqueous solution of $I_3^-/I^-$.

TABLE II

BAND GAPS, FLAT-BAND POTENTIALS, AND VALENCE BAND POSITIONS OF SEVERAL TRANSITION METAL DICHALCOGENIDES

| | $E_g$ (eV)[a] | $E_{FB}$ (V vs SCE) | $E_{VB}$ (V vs SCE) |
|---|---|---|---|
| $MoS_2$ | 1.17[b] | +0.21[c] | +1.29[c] |
| $MoSe_2$ | 1.06[b] | +0.01[c] | +0.94[c] |
| $WS_2$ | 1.3[d] | −0.2[d] | +1.1[d] |
| $WSe_2$ | 1.16[b] | −0.35[c] | +0.65[c] |
| $ReS_2$ | 1.32[e] | 0.0[f] | — |
| $ReSe_2$ | 1.17[e] | −0.2[f] | — |

[a] Lowest-energy indirect optical band gap.
[b] Reference (*14*).
[c] Reference (*13*).
[d] Reference (*22*).
[e] This work.
[f] Here $E_{FB}$ is taken to be the onset of photocurrent in an aqueous solution of $I_3^-/I^-$ (pH 1). These values indicate that the trend in $ReS_2$ and $ReSe_2$ is the same as in the other dichalcogenides (see text).

There are some general differences which can be observed when comparing the photoelectrochemical characteristics of the transition metal dichalcogenides with other semiconductors. Kung *et al.* (*32*) showed, for several *n*-type transition metal oxides, that the flat-band potential generally becomes more positive as the band gap decreases. The rationalization for this is that the valence band energy is determined primarily by $O^{2-}$ anions and is relatively constant. Thus, in *n*-type oxides with smaller band gaps, the conduction band must be more positive on the electrochemical scale, resulting in more positive flat-band potentials.

The characteristics of several transition metal dichalcogenides are listed in Table II. It can be observed that the band gaps of the diselenides are generally smaller than those of the corresponding disulfides. However, the flat-band potentials of the diselenides are more negative than the corresponding disulfides. Results from this work indicate that $ReS_2$ and $ReSe_2$ follow this same trend. Hence, the observations made for *n*-type oxide semiconductors do not apply to the transition metal dichalcogenides. The values listed in Table II indicate that both the metal and the anion affect the position of both the valence band and the conduction band. Thus, for the transition metal dichalcogenides, the valence band is not fixed solely by the anion.

It has been suggested (*1–7*) that both the valence band and the conduction band of the transition metal dichalcogenides are primarily *d* in character. Absorption of photons with energy greater than the band gap would therefore result in *d–d* transitions, which would not tend to break metal–anion bonds. This explains the enhanced stability of these materials over other semiconductors with more polar bonding (such as CdS and GaAs) in which promotion of an electron from the valence band to the conduction band tends to break metal–anion bonds, resulting in photocorrosion. $ReS_2$ and $ReSe_2$ showed good stability with reproducible current–potential characteristics over several experiments on the same crystal. This suggests that the photoeffect observed in $ReS_2$ and $ReSe_2$ single crystals is due to *d–d* transitions.

## Summary and Conclusions

Large single crystals of $ReS_2$ and $ReSe_2$ were grown by chemical vapor transport, and several of their properties were investigated. Both were found to be *n*-type semiconductors with resistivities in the range of 1–10 ohm-cm. Photoelectrochemical measurements in aqueous solutions of $I_3^-/I^-$ resulted in high photocurrent densities, with $ReSe_2$ being the more efficient photoelectrode. Analysis of their optical absorption spectra resulted in lowest-energy indirect optical band gaps of 1.32(5) eV for $ReS_2$ and 1.17(5) eV for $ReSe_2$. Photoelectrochemical spectral response measurements resulted in a measured lowest-energy indirect optical band gap of 1.4 eV for $ReS_2$ which is in close agreement with that measured from optical absorption.

The photoelectrochemical properties of $ReS_2$ and $ReSe_2$ were observed to follow some trends found in other transition metal chalcogenides. In general, the diselenides have smaller band gaps and more negative flat-band potentials than the corresponding disulfides. It has also been observed that both the metal and the anion have an effect on the positions of the valence band and the conduction band. Thus, the transition metal dichalcogenides exhibit a fairly wide range of photoelectrochemical characteristics.

## Acknowledgments

The authors thank GTE Laboratories, Inc. of Waltham, Massachusetts, and the National Science Foundation (DMR-82-03667) for the support of James V. Marzik. Acknowledgment is also made to the National Science Foundation (DMR-82-03667) for the support of Kirby Dwight, and to Brown University's Materials Research Laboratory which is funded through the National Science Foundation.

## References

1. H. TRIBUTSCH, *Z. Naturforsch. A.* **32,** 972 (1977).
2. H. TRIBUTSCH, *Ber. Bunsenges. Phys. Chem.* **81,** 361 (1977).
3. H. TRIBUTSCH AND J. C. BENNETT, *J. Electroanal. Chem.* **81,** 97 (1977).
4. H. TRIBUTSCH, *J. Electrochem. Soc.* **125,** 1086 (1978).
5. J. GOBRECHT, H. TRIBUTSCH, AND H. GERISCHER, *J. Electrochem. Soc.* **125,** 2085 (1978).
6. H. TRIBUTSCH, *Ber. Bunsenges. Phys. Chem.* **82,** 169 (1978).
7. J. GOBRECHT, H. GERISCHER, AND H. TRIBUTSCH, *Ber. Bunsenges. Phys. Chem.* **82,** 1331 (1978).
8. W. KAUTEK, H. GERISCHER, AND H. TRIBUTSCH, *Ber. Bunsenges. Phys. Chem.* **83,** 1000 (1979).
9. L. F. SCHNEEMEYER AND M. S. WRIGHTON, *J. Amer. Chem. Soc.* **101,** 6496 (1979).
10. H. J. LEWERENZ, A. HELLER, AND F. J. DISALVO, *J. Amer. Chem. Soc.* **102,** 1877 (1980).
11. S. MENEZES, F. J. DISALVO, AND B. MILLER, *J. Electrochem. Soc.* **127,** 1751 (1980).
12. L. F. SCHNEEMEYER, M. S. WRIGHTON, A. STACY, AND M. J. SIENKO, *Appl. Phys. Lett.* **36,** 701 (1980).
13. W. KAUTEK AND H. GERISCHER, *Ber. Bunsenges. Phys. Chem.* **84,** 645 (1980).
14. W. KAUTEK, H. GERISCHER, AND H. TRIBUTSCH, *J. Electrochem. Soc.* **127,** 2471 (1980).
15. F.-R. F. FAN, H. S. WHITE, B. L. WHEELER, AND A. J. BARD, *J. Amer. Chem. Soc.* **102,** 5142 (1980).
16. C. P. KUBIAK, L. F. SCHNEEMEYER, AND M. S. WRIGHTON, *J. Amer. Chem. Soc.* **102,** 6898 (1980).
17. L. F. SCHNEEMEYER AND M. S. WRIGHTON, *J. Amer. Chem. Soc.* **102,** 6964 (1980).
18. D. CANFIELD AND B. A. PARKINSON, *J. Amer. Chem. Soc.* **103,** 1279 (1981).
19. G. S. CALABRESE AND M. S. WRIGHTON, *J. Amer. Chem. Soc.* **103,** 6273 (1980).
20. H. S. WHITE, F.-R. F. FAN, AND A. J. BARD, *J. Electrochem. Soc.* **128,** 1045 (1981).
21. G. NAGASUBRAMANIAN AND A. J. BARD, *J. Electrochem. Soc.* **128,** 1055 (1981).
22. J. A. BAGLIO, G. S. CALABRESE, E. KAMIENIECKI, R. KERSHAW, C. P. KUBIAK, A. J. RICCO, A. WOLD, M. S. WRIGHTON, AND G. ZOSKI, *J. Electrochem. Soc.* **129,** 1461 (1982).
23. W. KAUTEK AND H. GERISCHER, *Surface Sci.* **119,** 46 (1982).
24. H. TRIBUTSCH, *J. Electrochem. Soc.* **128,** 1261 (1981).
25. H. TRIBUTSCH, *Faraday Discuss. Chem. Soc.* **70,** 190 (1981).
26. J. V. MARZIK, R. KERSHAW, K. DWIGHT, AND A. WOLD, *J. Solid State Chem.* **44,** 382 (1982).
27. J. C. WILDERVANCK AND F. JELLINEK, *J. Less-Common Met.* **24,** 73 (1971).
28. N. W. ALCOCK AND A. KJEKSHUS, *Acta Chem. Scand.* **19,** 79 (1965).
29. R. KERSHAW, M. VLASSE, AND A. WOLD, *Inorg. Chem.* **6,** 1599 (1967).
30. L. J. VAN DER PAUW, *Philips Res. Rep.* **13,** 1 (1958).
31. F. P. KOFFYBERG, K. DWIGHT, AND A. WOLD, *Solid State Commun.* **30,** 433 (1979).
32. H. H. KUNG, H. S. JARRETT, A. W. SLEIGHT, AND A. FERRETTI, *J. Appl. Phys.* **48,** 2463 (1977).